THE PHENIX EXPERIMENT

A.V.Khanzadeev, V.G.Riabov, V.M.Samsonov

1. Physics goals and general description

Ultra-relativistic heavy ion collisions offer the unique opportunity to probe highly excited dense nuclear matter under controlled laboratory conditions. The compelling driving force for such studies is the expectation that an entirely new form of matter may be created from such reactions – Quark Gluon Plasma (QGP) – a deconfined state of quarks and gluons. Such a form of matter presumably existed in the early Universe until it hadronized at an age of ten microseconds. The quark-gluon plasma has yet to be observed unambiguously, although there have been interesting effects of high density nuclear matter observed in the AGS and SPS experiments. This stimulated studies using relativistic heavy ions at significantly higher energies at the Relativistic Heavy Ion Collider and the Large Hadron Collider.

The Relativistic Heavy Ion Collider (RHIC) at Brookhaven National Laboratory (BNL), USA, which started regular operation in June 2000, is the first colliding-type accelerator dedicated to the heavy-ion studies. A layout of RHIC acceleration complex is shown in Fig. 1.

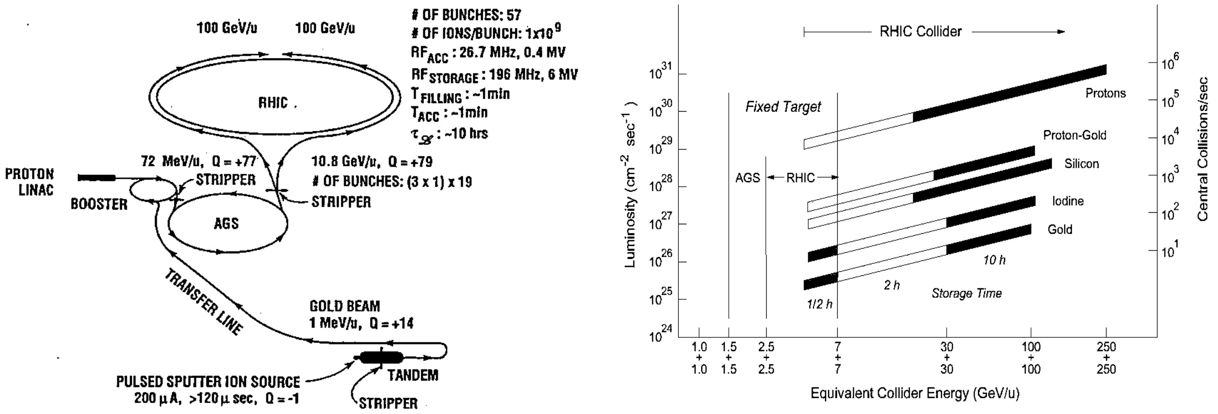

Fig. 1. RHIC accelerator complex at BNL (left). The RHIC luminosity and number of central collisions per second for impact parameters less than 1 fm (right)

Nuclear beams are accelerated from the tandem Van de Graff accelerator through a transfer line into the AGS Booster synchrotron and then into the AGS, which serves as an injector for RHIC. RHIC will accelerate and collide ions from protons up to the heaviest nuclei over a range of energies, up to 250 GeV for protons and 100 GeV/nucleon for Au nuclei. Fig. 1 summarizes the capabilities of the accelerator. In addition to the colliding beams shown in Fig.1, plans are underway to inject and accelerate polarized protons at RHIC in order to study the spin content of the proton. The RHIC experimental program is essentially defined with two large detectors (STAR and PHENIX) and two smaller ones (PHOBOS and BRAMS) located in four (out of six) interaction points.

The PHENIX (Pioneering High Energy Nuclear Interaction eXperiment) experiment has been designed to measure a broad variety of signals from both heavy ion and polarized proton-proton collisions. Table 1 summarizes the physics quantities measured by PHENIX and their relationship to physics objectives. The strategy of the PHENIX collaboration (45 laboratories from 12 countries) is to measure as many potential signatures of the QGP as possible as a function of well-defined common variables such as an impact parameter or a pseudorapidity density. The PHENIX focuses on measurements of lepton pairs (dielectrons and dimuons) and photon production and has the capability of measuring hadrons in a limited range of pseudorapidity. The leptons arise from the plasma phase and probe it directly, whereas the more copious hadrons provide the complementary information about the hadronization phase transition. Two basic properties of the plasma, the Debye screening of quantum chromodynamics (QCD) interactions and the chiral symmetry restoration, are significant elements of these measurements. The thermal radiation of a hot gas is also very important since it characterizes the temperature of the system formed in these collisions.

Deconfinement of quarks and gluons in QGP is closely related to the Debye screening of the QCD potential. If the J/Ψ radius is longer than the screening length, then a $c\bar{c}$ pair would not be able to form a bound state due to the Debye suppression of the long-range term of the $c\bar{c}$ potential and, thus, the J/Ψ production is suppressed. The degree of suppression depends strongly on the relative size difference between the meson radius and the screening length. Because $r(\Psi^{'}) = 0.51$ fm > $r(J/\Psi) = 0.25$ fm > $r(\Upsilon) = 0.13$ fm, one can expect that the $\Psi^{'}$ must melt first, then the J/Ψ, and finally the Υ. The J/Ψ can be measured in the midrapidity region by dielectrons, and the J/Ψ, $\Psi^{'}$ and Υ at forward angles by dimuons.

Table 1

Physics issues related to QGP to be measured at PHENIX

QGP Physics Issues	Probes
Debye Screening of QCD Interactions $r(\Upsilon) = 0.13$ fm < $r(J/\Psi) = 0.25$ fm < $r(\Psi^{'}) = 0.51$ fm [1]: $J/\Psi \to e^+e^-$ at $y \approx 0$, $J/\Psi \to \mu^+\mu^-$ at $y \approx 2$, $\Psi^{'}$, $\Upsilon \to \mu^+\mu^-$ at $y \approx 2$.	Electrons Muons
Chiral Symmetry Restoration Mass, Width, Branching Ratio: $\phi \to e^+e^-$, K^+K^- with $\Delta m \leq 5$ MeV [1].	Electrons Hadrons
Thermal Radiation of Hot Gas Prompt γ, prompt $\gamma^* \to e^+e^-$ [2].	Photons, electrons
Deconfinement: Nature of the Phase Transition First-order: Entropy Jump $\to$ Second rise in the $\langle p_t \rangle$ spectra of π, K, p. Second-order: Fluctuation $\to N(\pi^0)/N(\pi^+ + \pi^-)$, $d^2N/d\eta d\varphi$ [3].	Hadrons Hadrons, photons
Strangeness and Charm Production Production of K^+, K^-, K_L^0 [4]. $\phi \to e^+e^-$, K^+K^- at $y \approx 0$ [5], $\phi \to \mu^+\mu^-$ at $y \approx 2$. D-meson: $e\mu$ coincidence [6].	Hadrons Electrons Muons
Jet Quenching High p_t jets *via* leading particle spectra [7].	Hadrons
Space-Time Evolution HBT correlations for $\pi\pi$ and KK [8].	Hadrons

Because the mass of the ϕ-meson is close to twice the kaon mass, and because both ϕ and K could be distorted in the quark-gluon plasma, it was predicted that a change would occur in the branching ration between leptonic and hadronic channels, the mass and width of the ϕ-meson. A high resolution ϕ-spectroscopy is required to study these points. The ϕ-meson should be measured using both electron and hadron channels.

The thermal radiation from a hot gas has been a subject of controversy for many years. Recently, a consensus among theorists seems to be that the gluon content is high at an early stage of the QGP and an enhancement must be expected in the region of m_T (or p_t for photons) greater than 2–3 GeV. This topic can be investigated using photon measurement capabilities at PHENIX. Neutral mesons, such as π^0 and η, are also measured through the photon channel.

Electron and muon pairs should be measured to study properties of the vector mesons (*e.g.* mass, width, yield) and to study continuum spectra in different regions of rapidity and mass. The electron-muon

---

[1] T.Matsui *et al.*, Phys. Lett. **B178**, 416 (1986); K.Kajantie *et al.*, Phys. Rev. **D34**, 2746 (1986).
[2] E.Shuryak *et al.*, Phys. Lett. **B78**, 15 (1978); M.Kataja *et al.*, Phys. Rev. **D34**, 2755 (1986).
[3] P.Pisarski *et al.*, Phys. Rev. **D29**, 338 (1984); J.Bjorken *et al.*, Int J. Mod. Phys. **A7**, 4189 (1992).
[4] S.Margetis *et al.*, Ann. Rev. Nucl. Part. Sci. **50**, 299 (2000).
[5] D.Lissauer *et al.*, Phys. Lett. **B253**, 15 (1991).
[6] B.Miller *et al.*, Phys. Rev. Lett. **68**, 2437 (1992).
[7] M.Gyulassy *et al.,* Phys. Lett. **B243**, 432 (1990).
[8] S.Pratt *et al.*, Phys. Rev. **C33**, 1314 (1986); J.Ellis *et al.,* Phys. Lett. **B233**, 223 (1989).

coincidence probes charm production and aids in understanding the shape of the continuum dilepton spectrum. The detection and identification of charged hadrons allow the study of the p_t distributions, the production of antinuclei, the ϕ-meson (*via* K^+K^- decay), jets, and Hanbury-Brown-Twiss (HBT) correlations. The order of the phase transition, flow effects, shadowing and jet-quenching, possible fluctuations are also promising candidates for the study of QGP phase transition at PHENIX. As one can see from Table 1, the simultaneous measurements of leptons, photons and hadrons as well as the particle identification are important elements of the PHENIX experiment.

The PHENIX detector consists of a central spectrometer with an axial magnetic field ($\int \mathrm{Bdl} \sim 0.78$ T·m) and two forward muon spectrometers with a roughly radial field. A detailed description of the detector can be found elsewhere. Two arms of the central spectrometer are separated by 45° azimuth (ϕ). Charged and neutral particles are detected by this two-arm spectrometer, each arm subtending 90° in ϕ and ±0.35 units in pseudorapidity η, roughly equivalent to polar angle (θ) acceptance of ±20° centered at θ equal to 90°. The solid angle of each arm is 0.94 sr. Particle tracking is performed with the help of three subsystems: Pad Chambers (PC), Drift Chambers (DC) and Time-Expansion Chamber (TEC). An electron identification is performed by detection of the Cherenkov radiation by the Ring Imaging Cherenkov Counters (RICH), by measurement of the energy loss in the TEC and time-of-flight and electromagnetic showers in the PbSc calorimeter. Within the aperture for the electron measurement there are detector subsystems with limited acceptance for photons, using the PbGl calorimeter ($\Delta\phi = 45°$, $\Delta\eta = \pm 0.35$), and for charged hadrons, using a high precision Time-of-flight (TOF) array ($\Delta\phi = 45°$, $\Delta\eta = \pm 0.35$). The PbSc also measures photons with an energy resolution close to that achieved in PbGl. Together they comprise the PHENIX electromagnetic calorimeter (EMCal). Two muon spectrometers covering the full azimuth for $1.1 < |\eta| < 2.4$ are used to track and identify muons. Each muon spectrometer contains a magnet, that produces a roughly radial field, and uses cathode strip chambers in three stations for tracking (μTr) and five layers of Iarocci tubes interleaved with an iron absorber for muon identification (μID). The global event characterization is achieved *via* multiplicity and vertex detector (MVD) consisting of silicon strips and pads covering $|\eta| < 2.5$. The front-end electronics for all subsystems are clocked synchronously with the beam crossing frequency of 9.4 MHz. A set of Level-1 and Level-2 triggers derived from various subsystems are used to initiate readout of the entire detector through a pipelined high bandwidth data acquisition system.

Fig. 2. General view of the Drift Chamber

The innermost part of each central spectrometer arm is the DC (see Fig. 2) designed and produced at PNPI in collaboration with Stony Brook University [1]. The DC consists of 40 planes of wires arranged in 80 drift cells placed cylindrically symmetric with respect to beam line. Each DC spans 90° in ϕ, has a radial-sensitive region from 2.02 to 2.46 meters and covers $-80 < z < 80$ cm (the coordinate system originates at the centre of the central spectrometer magnet and has z-axis along the beam). More than 3000 sensitive wires electrically disconnected in the middle and readout independently from both sides sample several points along each charged particle trajectory. The DC use a gas mixture of 50% argon and 50% ethane at atmosphere pressure that results in an electron drift velocity of ~ 52 μm/ns under operational high voltage regime. The original direction of the particles is not measured, thus the particle momentum is determined by the bend angle of the track with respect to a straight trajectory coming from the interaction point. Good single wire (σ ~ 160 μm) and double track (σ ~ 1.5-2 mm) resolution in the plane perpendicular to The beam, which coincides in this case with the main bend plane, makes this device ideal for the momentum reconstruction with a good resolution in the environment of very high particle density. Several layers of stereo wires allow DCs to reconstruct 3-D spatial position of tracks that significantly simplifies the pattern recognition.

Schematic view of the PHENIX detector as it was during the summer run of 2000 is shown in Fig. 3. Muon arms as well as MVD were partially installed but did not contribute in the common data stream and as a consequence could not be used for data analysis. All other subsystems were 25−100% instrumented and readout. Two pairs of Zero Degree Calorimeters (ZDC) and Beam-Beam Counters (BBC) were used to derive the trigger and the off-line event selection. ZDC are small transverse-area hadron calorimeters that measure neutron energy within a 2 mrad ($|\eta|>6$) cone around the beam direction and are located at ±18.25 m from the centre of the interaction region. The BBC comprise two arrays of 64 photomultipliers each equipped with quartz Cherenkov radiators. The BBC are located around the beam direction at ±1.44 m from the centre of the interaction region covering the full 2π azimuth and the range $\eta = \pm$ (3.0–3.9). The primary interaction trigger is generated by a coincidence between the two BBC with at least two photomultipliers fired in each of them and a requirement on the collision vertex position, usually $|z| \leq 20$ cm. Based on detailed simulations of the BBC, this trigger reflects 92±2(syst)% of the nuclear interaction cross section of 7.2 barns. Another trigger is generated by a coincidence between the two ZDC, each one with an energy signal larger than 10 GeV. This trigger reflects the nuclear interaction plus the mutual Coulomb dissociation cross section. Most BBC triggers (97.8%) also satisfy the ZDC trigger requirement. Event classes by centrality were defined by cuts in the space of BBC versus ZDC analog response and refer to percentiles of the total interaction cross section. A simulation of the BBC and ZDC response was used to account for the effect of physics and detector fluctuations in the definition of these

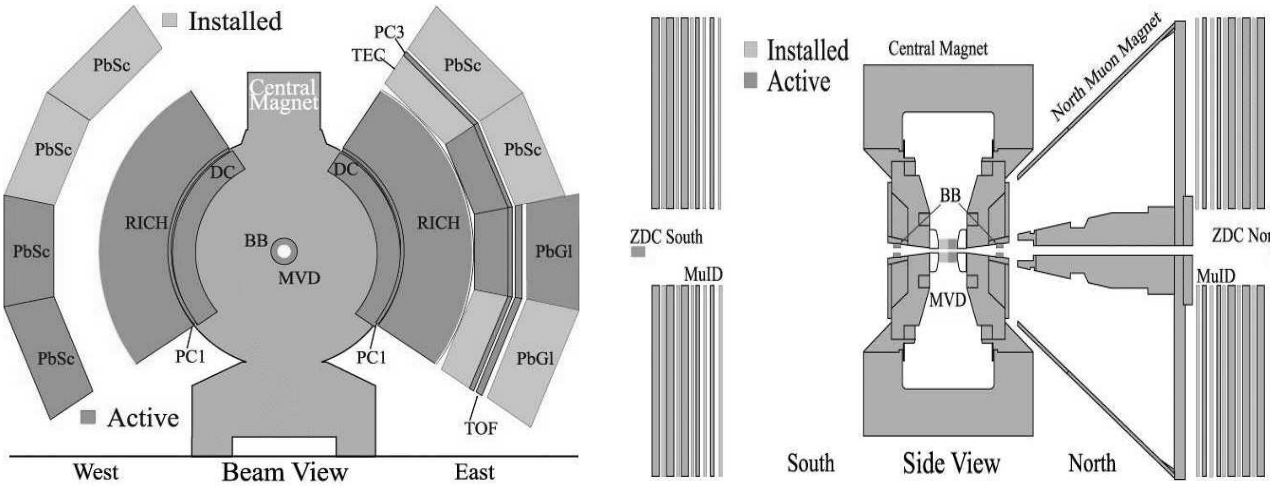

Fig. 3. Detectors installed/active for the first run of RHIC in summer of 2000

event classes and to relate them *via* a Glauber model to the number of participating nucleons N_p and of the binary collisions N_c [9]. For the first physical run PHENIX collaboration considered as main goals:

- Incorporating all subsystems into the one detector and its implementation to the common PHENIX infrastructure.
- Measuring some global parameters of ion-ion interactions.

A total amount of approximately 5M events of gold-gold collisions was recorded at $\sqrt{s_{NN}}$ =130 GeV.

[9] M.Chiu, PHENIX analyses note an018, 2000. 16 p.

2. Global observables

Global variables such as pseudorapidity charged particle ($dN_{ch}/d\eta|_{\eta=0}$) and transverse energy ($dE_T/d\eta|_{\eta=0}$) densities are important for the characterization of high-energy nuclear collisions. They constrain theoretical models, help to discriminate among various mechanisms of particle production and allow deriving information about the initial conditions. Fig. 4 shows the multiplicity [2] and transverse energy [3] per pair of N_p versus N_p measured by PHENIX. One can see that the extrapolation to $N_p = 2$ of measured $dN_{ch}/d\eta|_{\eta=0}$ points is in agreement with the UA5 data for $p\bar{p}$. Results obtained by WA98 at $\sqrt{s_{NN}}$ = 17.2 GeV are shown also. The curves represent a fit to the data points with $dX/d\eta \propto N_p^{\alpha}$, where X means N_{ch} or E_T. For $dN_{ch}/d\eta$ one finds $\alpha = 1.16 \pm 0.04$ for PHENIX whereas $\alpha = 1.07 \pm 0.04$ and $\alpha = 1.05 \pm 0.05$ for WA98 and WA97/NA57, respectively. For $dE_T/d\eta$ the PHENIX value is $\alpha = 1.13 \pm 0.05$ compared to $\alpha = 1.08 \pm 0.06$ for WA98. One can conclude that at RHIC energies both measured quantities show a consistent increase with centrality, with an α value evidently larger than unity, whereas at the SPS energy α was found to be very close to 1.

Fig. 4 compares the measured $dN_{ch}/d\eta$ with the theoretical predictions of the EKRT [10] saturation model and HIJING [11]. The increase of $dN_{ch}/d\eta$ with N_p is in contrast to the prediction of the EKRT model and in qualitative agreement with HIJING, however the latter underestimates the yield by ~ 15%. Following HIJING, one can assume that the increase is due to “hard” processes that scale with N_c. In the framework of the HIJING model the “hard” contribution grows from ~30% for the 45–50% centrality bin to ~50% for the most central bin (0–5%).

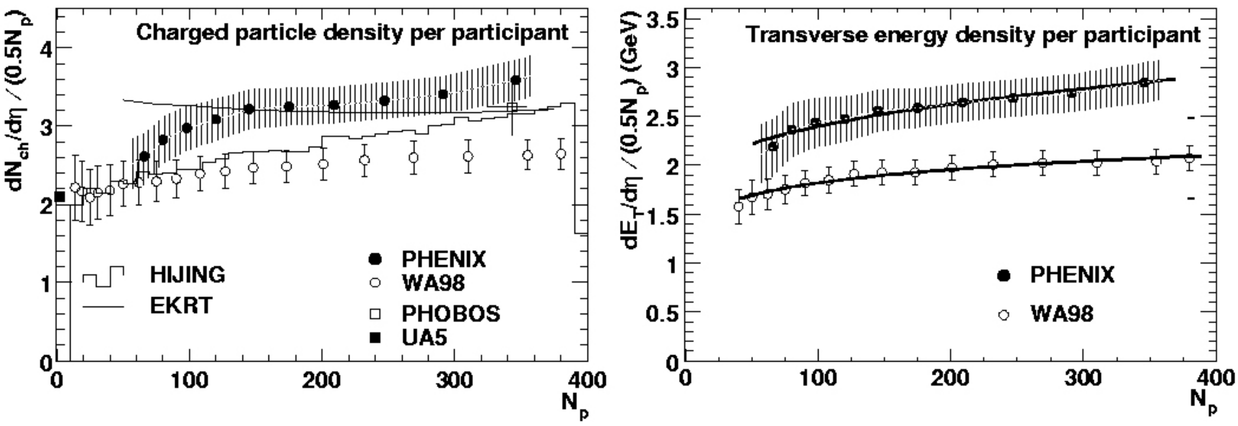

Fig. 4. The charged-particle pseudorapidity density (left) and the transverse energy pseudorapidity density (right) per participant pair versus the number of participants. The band in each figure indicates the systematic errors

In the case of energy density, when calculated following the Bjorken prescription [12], the value of 4.6 GeV/fm^3 is roughly 60% larger than that found at the SPS [13]. However the ratio $\langle E_T\rangle/\langle N_{ch}\rangle$ of the transverse energy per charged particle stays constant, equal to 0.8 GeV over a broad range of centralities, as was observed by CERN experiment WA98. Moreover, this ratio stays also constant as a function of $\sqrt{s_{NN}}$ from AGS to SPS and up to RHIC energies.

[10] K.Eskola *et al.*, Nucl. Phys. **B570**, 379 (2000).
[11] X.Wang *et al.,* Phys. Rev. **D44**, 3501 (1991).
[12] J.D.Bjorken, Phys. Rev. **D27**, 140 (1983).
[13] T.Alber *et al.*, Phys. Rev. Lett. **75**, 3814 (1998).

3. Production at high transverse momentum

Hard-scattered partons fragment into jets of hadrons and so manifest themselves as hadrons at high transverse momentum (p_t). Thus the influence of the nuclear collision medium on hard-scattered partons can be observed by measuring the spectra of high-p_t hadrons. It has been predicted that scattered partons lose energy in the dense medium through gluon bremsstrahlung, an effect known as “jet quenching”. This would have many observable consequences, the simplest of which would be a depletion in the yield of single hadrons at high p_t.

The p_t distributions for charged hadrons and neutral pions for two centrality classes defined as 0–10% (most central) and 60–80% fraction of the geometrical Au+Au cross section are presented in Fig. 5 [4]. The data are compared to reference spectra from *pp* collisions scaled by the number of binary collisions N_c. For p_t > 2 GeV/c, where hard scattering processes are expected to dominate the hadron production, the binary-scaling prediction agrees quite well with the data from peripheral collisions, for both charged and neutral particles. For central collisions, however, the data lie noticeably below the binary-scaling prediction for both spectra. This depletion is quite striking, since the production of high-p_t hadrons in *p*+A collisions at fixed target energies is known to be enhanced compared to the binary-scaling expectation for p_t > 2 GeV/c, a behaviour generally termed the “Cronin effect” [14]. A similar enhancement has also been observed in heavy ion collisions at lower energies. The central-to-peripheral ratio shown in Fig. 5 is useful complement, since in the limit of point-like scaling it should be unity. This ratio obtained by PHENIX is significantly below 1.0 at all observed p_t both for charged hadrons and neutral pions, indicating a suppression of the yield per nucleon-nucleon collision in central collisions relative to peripheral ones. The difference between two ratios corresponding to charged hadrons and neutral pions implies that the h/π ratio is larger in central collisions than in peripheral, although within the systematic errors not inconsistent with that seen at p_t ~ 2 GeV/c for charged pions. The suppression in the central Au+Au collisions is in a qualitative agreement with the predictions of the effect of significant energy loss by scattered partons transversing a dense collision medium.

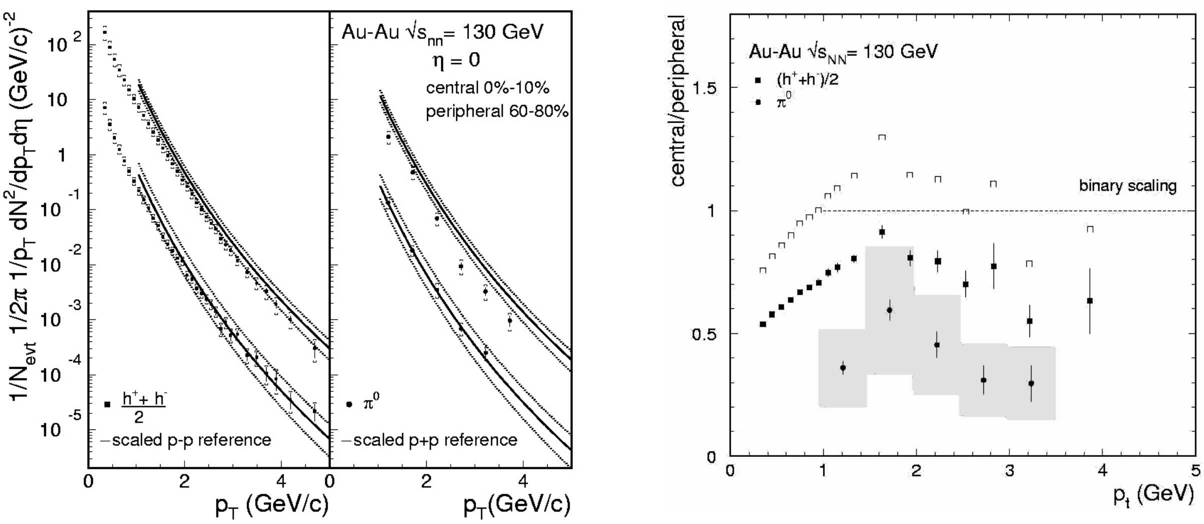

Fig. 5. The yields per event at mid-rapidity for charged hadrons and neutral pions (left) as a function of p_t for two centrality classes. The error bars indicate the statistical errors, the surrounding brackets indicate the systematic errors. Shown for reference are the yields per *pp* collision for charged hadrons and neutral pions respectively, each scaled by N_c for the class. The bands indicate both the uncertainty in the *pp* data and in the determination of N_c. Ratio of yield per event in central versus peripheral Au+Au collisions, with each divided by N_c for that class (right)

[14] D.Antreasyan *et al.*, Phys. Rev. **D19,** 764 (1979).

4. Identified hadrons

Transverse momentum spectra of identified π^+, π^-, K^+, K^-, p and $\bar{p}$ were measured by the PHENIX experiment over a broad momentum range. Normalized minimum bias p_t spectra for these particles are shown in Fig. 6 [5]. The lower p_t cutoffs were imposed due to a loss of acceptance and tracking efficiency, while the higher p_t cutoff values for π^+, π^- and K^+, K^- are dictated by the detector capability in π/K mass separation. The shape of the spectra clearly depends on the particle species, with pions having the lowest $\langle p_t \rangle$ and protons and anti-protons having the highest. The pion and kaon $\langle p_t \rangle$ is similar to that in $p\bar{p}$ collisions, and within errors is independent of N_p. The observed $\langle p_t \rangle$ for protons and anti-protons is higher than in $p\bar{p}$ collisions and seems to increase logarithmically with N_p. The dependence of the local slopes increases with both centrality and with particle mass, consistent with expectations from radial flow.

Particle ratios at high p_t contain direct information about initial conditions, since the production of high p_t particles is dominated by the jet production [6]. As an example, the $p/\bar{p}$ ratio at high p_t may provide information on the predicted difference between the energy lost by high p_t quarks and gluons.Figs. 7, 8 show measured K^+/K^- and $p/\bar{p}$ ratios as a function of the transverse momentum and number of participants for minimum bias data. Within errors, the K^+/K^- and $p/\bar{p}$ ratios do not depend on p_t over the measured range. For kaons ratio is found to be 1.08 ± 0.03(stat) $\pm$ 0.22(syst), which is extracted by averaging over the p_t range $0.8 < p_t < 1.6$ GeV/c. A strong suppression of the $p/\bar{p}$ ratio at high p_t due to jet quenching was suggested by Wang [15]. The $p/\bar{p}$ ratio for minimum bias collisions is found to be 0.63 ± 0.01(stat) $\pm$ 0.07(syst), which is extracted by averaging over the p_t range $0.8 < p_t < 3.0$ GeV/c. This value signifies that the central region in heavy ion collisions at RHIC is meson-dominated, as distinct from the baryon-dominated case at the SPS and lower energies, where the ratio is never larger than ~ 0.1. No centrality dependence of K^+/K^- or $p/\bar{p}$ ratio is observed. A similar lack of centrality dependence was observed in experiments at SIS [16], AGS [17] and SPS [18].

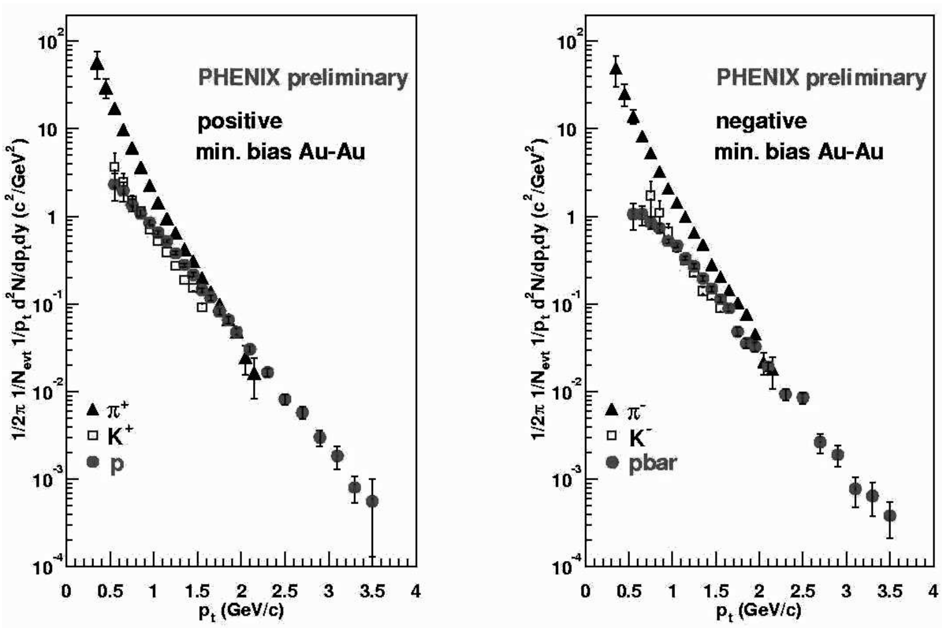

Fig. 6. Normalized minimum bias transverse momentum spectra for positive (left) and negative (right) identified particles. The error bars are composed of statistical errors and systematic errors associated with acceptance and decay corrections. There is an additional 20% systematic error with the overall normalization

[15] X.Wang, Phys. Rev. **C58**, 2321 (1998).
[16] M.Menzel *et al*., Phys. Lett. **B495**, 26 (2000).
[17] L.Ahle *et al*., Phys Rev**. C58**, 3523 (1998).
[18] S.Kabana *et al*., Nucl. Phys. **A661**, 177 (1999).

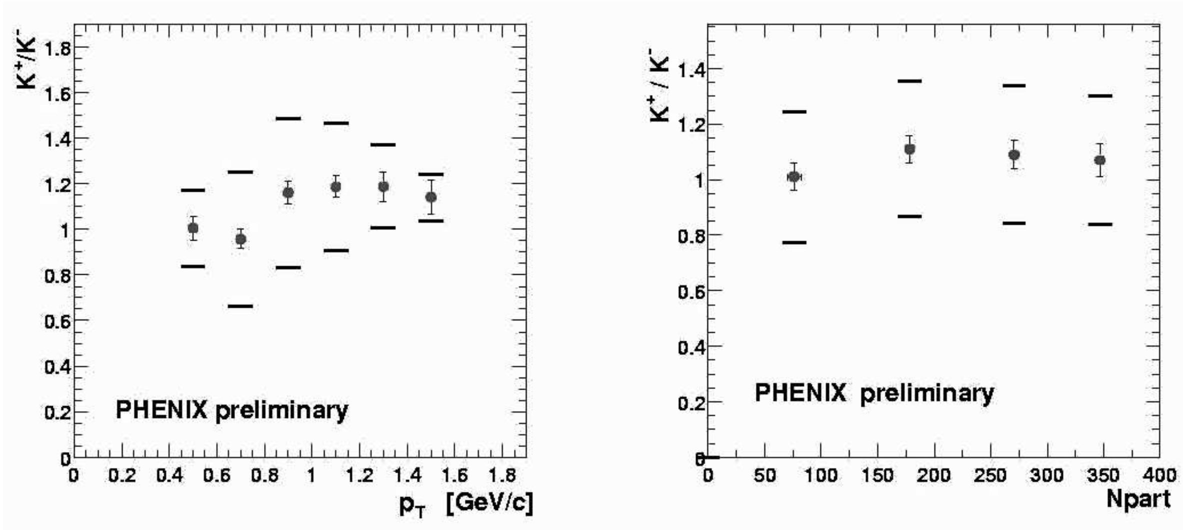

Fig. 7. K^+/K^- ratio for minimum bias Au+Au collisions as a function of transverse momentum and number of participants

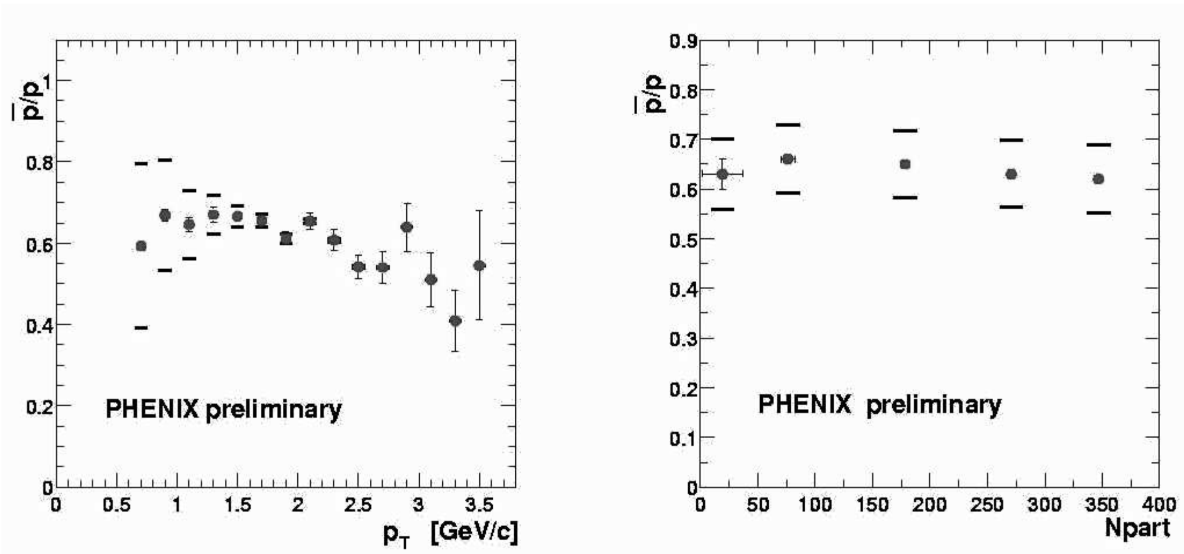

Fig. 8. $p\bar{p}$ ratio for minimum bias Au+Au collisions as a function of transverse momentum and number of participants

Charged pion pairs in the central arms have also been used to perform an HBT analysis, which allows a measurement of the space-time extent of heavy ion collisions. Fig. 9 shows the Coulomb corrected correlation functions for π^- pairs measured in the EMCal analysis overlaid with the resulting fit [7]. The results of the fit are shown in Table 2 along with the results from the π^+ analysis from the EMCal and π^+/π^- analysis utilizing the TOF. The results do not indicate an especially large size of the source compared to measurements at lower energies, and resulting naively calculated lifetime deduced from these measurements is consistent with zero. However, a stronger collective flow will shorten the effective source and lifetime measured by HBT.

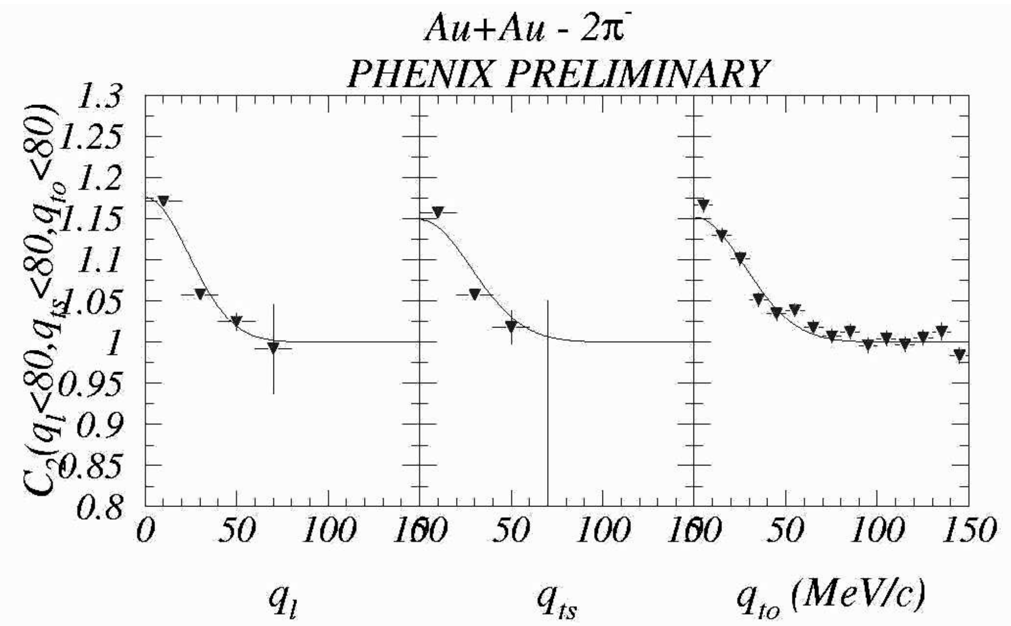

Fig. 9. Correlation function for π^- pairs from the EMCal analysis. The one-dimensional correlation function is averaged over the lowest 80 MeV/c in the other momentum differences

Another global feature of hadronic production is the azimuthal pattern of emission, as parameterized by an elliptic flow. The elliptic flow, which is a hadronic observable sensitive to the early stages of system evolution, is the anisotropic emission of particles "in" or "out" of the reaction plane defined for non-central collisions by the beam direction and the impact parameter direction. The elliptic flow has its origin in the spatial anisotropy of the system when it is created in a non-central collision, and in particle rescattering in the evolving system which convert the spatial anisotropy to momentum anisotropy. Being dependent on rescattering, the elliptic flow is sensitive to the degree of thermalization of the system at this early time.

Table 2

Results of the Bertsch-Pratt fits to the identical pion pairs in the EMC and TOF analyses. Errors shown represent statistical uncertainties only; current systematic uncertainties are < 1fm

Data set	R_{Tout}, fm	R_{Tside}, fm	R_{Long}, fm	λ
EMC $\pi^+\pi^+$	4.4 ± 0.2	5.1 ± 0.6	5.9 ± 0.4	0.27 ± 0.02
TOF $\pi^+\pi^+$	6.2 ± 0.5	7.9 ± 1.1	4.0 ± 1.2	0.49 ± 0.05
EMC $\pi^-\pi^-$	5.1 ± 0.2	5.0 ± 0.6	5.9 ± 0.4	0.3 ± 0.02
TOF $\pi^-\pi^-$	5.5 ± 0.5	5.8 ± 1.5	6.7 ± 0.9	0.49 ± 0.06

PHENIX performed an elliptic flow analysis using charged particles with p_t > 200 MeV/c in the interval $|\eta| < 0.35$ [8]. The correlation function $C(\Delta\phi)$, where $\Delta\phi$ is the difference in azimuthal angle between two particles from the same event, was calculated using an event-mixing prescription to determine the background distribution, then fit to extract the v_2 coefficient: $C(\Delta\phi) \propto 1 + 2|v_1|^2\cos(\Delta\phi) + 2|v_2|^2\cos(2\Delta\phi)$. The second Fourier coefficient v_2 is commonly used to quantify the elliptic flow with respect to reaction plane. The measured by PHENIX dependence of v_2 on the transverse momentum and centrality is shown in Fig. 10. The elliptic flow at RHIC rises up to about 10% for the most peripheral collisions, a value which is more than 50% larger than at the SPS, indicating stronger early-time thermalization at the RHIC energy. Furthermore, the observed shape of the centrality dependence of the elliptic flow is similar to hydrodynamic calculations. Since these calculations assume a local thermal equilibrium at every space-time point in the collision zone, they are suggestive of the possibility that the rapid thermalization occurs in Au +Au collisions at RHIC. Such a notion is important for the task of establishing whether or not the QGP formation occurs at RHIC.

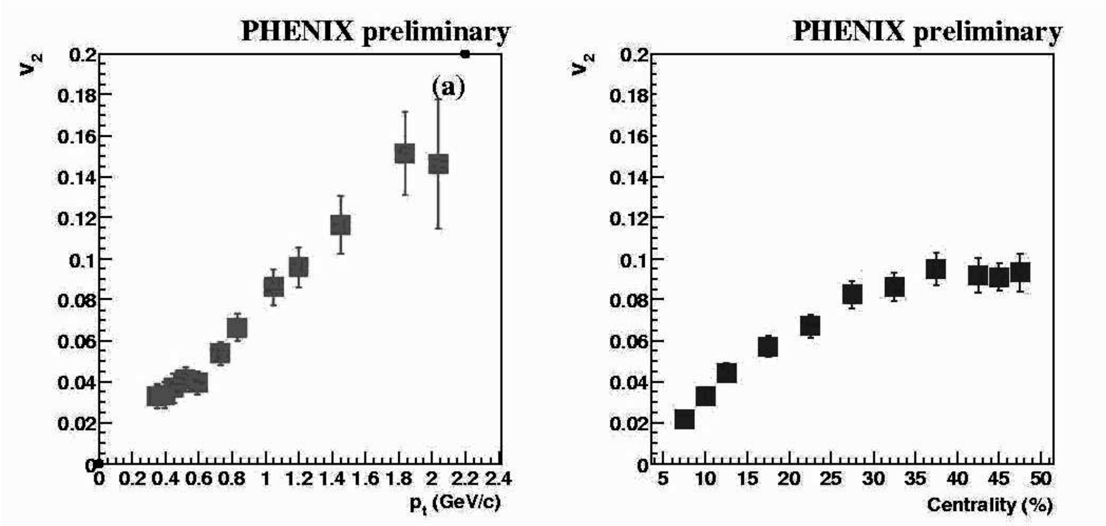

Fig. 10. Dependence of v_2 on momentum and centrality. Errors are statistical only

Future plans

In the oncoming RUN-2 at RHIC the complete aperture of the central arms will be available, much of the MVD will be instrumented, and entirely new spectrometer to measure muons will be deployed. These additions in aperture and in capability, coupled with significant upgrades to the data acquisition and triggering system, should result in a hundredfold or more increase in the event sample obtained from RUN-2.

The major goals of the PHENIX physics program remain unchanged (see Table 1): to measure phenomena from all timescales in Au+Au collisions, to correlate the greatest possible variety of such observables, and to characterize thereby the dense nuclear matter and search for the quark-gluon plasma. The only way to fulfil this program is a dramatic extension in PHENIX sensitivity to hard scattering and rare probes, both in heavy ion Au+Au collisions and in an accompanying and essential *pp* comparison run. These new measurements address some of the most pressing questions in heavy ion physics (charmonium production and suppression, energy loss of high p_t partons, direct photon production), while the *pp* comparison run will not only provide the requisite baseline data but also allow the first look at the gluon spin polarization *via* inclusive π^0 production. The sensitivity and flexibility of PHENIX, coupled with a steady increase in the RHIC luminosity, will provide an extensive characterization of the properties of heavy ions (Au) colliding at the highest energies yet observed. The first gold-gold collisions at full RHIC energy ($\sqrt{s}$ = 200 *A* GeV) have been detected by all experiments on 18th of July, 2001.

PNPI participants of the PHENIX collaboration: V.V.Baublis, V.A.Evseev, V.I.Ivanov, M.R.Kann, A.V.Khanzadeev, L.M.Kochenda, B.G.Komkov, P.A.Kravtsov, L.G.Kudin, V.V.Kuriatkov, V.D.Lebedev, D.G.Markushin, N.M.Miftakhov, V.G.Riabov, Yu.G.Riabov, E.V.Roschin, V.M.Samsonov, G.P.Solodov, V.I.Tarakanov, O.P.Tarasenkova, V.A.Trofimov, V.I.Vishnevskii, A.A.Vorobyov, E.A.Vznuzdaev.

References

[1] V.Riabov *et al.*, Nucl. Inst. Meth. **A419**, 363 (1998).
[2] K.Adcox *et al.*, Phys. Rev. Lett. **86**, 3500 (2001).
[3] K.Adcox *et al.*, Phys. Rev. Lett. **87**, 052301 (2001).
[4] C.David *et al.*, PHENIX analyses note an076, 2001, 13 p.
[5] J.Velkovska *et al.*, e-Print Archive nucl-ex/0105012, 2001. 4 p.
[6] H.Ohnishi, PHENIX analyses note an064, 2001. 4 p.
[7] S.Johnson, e-Print Archive nucl-ex/0104020, 2001. 4 p.
[8] L.Roy *et al.*, e-Print Archive nucl-ex/0105003, 2001. 4 p.